coatings

Article

Room Temperature Synthesis of Branched ZnO Nanowires Array with Tunable Morphology

Wei Zhao [1,2], **Hsiang-Shun Chang** [1,3], **Kefu Yao** [1,3] **and Yang Shao** [1,3,*]

[1] School of Materials Science and Engineering, Tsinghua University, Beijing 100084, China
[2] State Key Laboratory of New Ceramics and Fine Processing, Beijing 100084, China
[3] Key Laboratory for Advanced Materials Processing Technology, Ministry of Education, Beijing 100084, China
[*] Correspondence: shaoyang@tsinghua.edu.cn

Abstract: Herein, a novel method is proposed to synthesize B-ZnO NWA by simply immersing the Zn NWA in NaOH solution at room temperature (25 °C). Based on the systematic investigation of various factors that affect the growth of B-ZnO NWA, the growth mechanism of B-ZnO NWA is clarified. Guided by the growth mechanism, the control of the morphology of B-ZnO NWA is achieved by adjusting the pore structure of anodized aluminum oxide templates, hot-pressing parameters, NaOH concentration, solution temperature, and immersion time. In contrast to previous reports, the prepared B-ZnO NWA has hollow trunks, which can further increase the specific area of B-ZnO NWA. Considering the facile, environmental, and low-cost synthesis, the prepared B-ZnO NWA with tunable morphology has great prospects in a wide range of applications, especially those related to the conversion and utilization of solar energy, which are gaining increasing interest nowadays.

1. Introduction

ZnO has found wide applications in many fields due to its unique physicochemical properties [1–4] and morphological diversity [5]. Among numerous ZnO nanostructures, branched ZnO nanowires array (B-ZnO NWA) attracts great attention due to its large specific surface area, high volume filling ratio direct charge transport pathway, and efficient charge collection [3]. Favored by these advantages, B-ZnO NWA finds broad applications in the area of solar cells [6,7], photoelectrochemical water splitting [8,9], sensors [10,11], etc.

The synthetic methods of B-ZnO NWA can be divided into three categories. One-step synthesis of B-ZnO NWA was achieved through hydrothermal oxidation of Zn foil in 3.75 M ethylenediamine solution at 140 °C for 10 h [12]. Two-step synthesis of B-ZnO NWA was realized through an initial preparation of ZnO NWA and the subsequent growth of ZnO branches on ZnO NW through thermal-assisted pulsed laser deposition [13]. Three-step synthesis was the most common strategy to prepare B-ZnO NWA. It usually included the growth of ZnO NWA, the deposition of ZnO seeds [9] or metal catalysts [11] on ZnO NW, and the subsequent growth of ZnO branches [6,9,11,14,15]. These pioneering studies are of great importance as they have laid out a path toward higher efficiency of ZnO-based devices. However, the high temperature, environmental unfriendliness (organic additives), tedious procedures, and the loose morphology control of the existing methods hinder the further development of B-ZnO NWA.

In this paper, a novel method is proposed to prepare B-ZnO NWA via the immersion of Zn NWA in NaOH solution at room temperature (25 °C). Compared with the traditional methods, the proposed method is more facile, eco-friendly and energy-efficient. More importantly, the morphology of B-ZnO NWA can be well controlled by adjusting the pore structure of the anodic aluminum oxide (AAO) templates, hot-pressing parameters, NaOH concentration, solution temperature, and immersion time.

2. Materials and Methods

2.1. Materials

Zn foil (99.99%, thickness: 0.1 mm) was bought from Trillion Metals Co., Ltd (Beijing, China). Sodium hydroxide (NaOH, 99.9%) was obtained from Shanghai Aladdin Biochemical Technology Co., Ltd. (Shanghai, China) AAO templates were purchased from Shanghai Shangmu Technology Co., Ltd. (Shanghai, China). All materials were used as received without further purification in this work. The aqueous NaOH solution was prepared using deionized water.

2.2. Preparation of Zn NWA

The Zn NWA was prepared using the AAO template-assisted hot-pressing method [16]. Firstly, a Zn foil was cleaned through ultrasonication in acetone, ethanol, and deionized water, successively. Then, an AAO template was placed on top of a cleaned Zn foil (Φ = 5 mm) between two indenters that were made of high-temperature alloy (Inconel 718). The whole compression device was stabilized at 200 °C for 30 min before a pressure of 400 MPa was applied for a certain period. The temperature was maintained at 200 °C during the hot-pressing process. Afterwards, the sample was naturally cooled down to room temperature. Zn NWA was obtained by immersing the sample in 0.35 M NaOH solution at 25 °C for 60 min to remove the AAO template, followed by rinsing with 20 mL deionized water 3 times.

2.3. Preparation of B-ZnO NWA

B-ZnO NWA was obtained through a simple immersion process. Specifically, the Zn NWA was placed at the bottom of a glass sample vial, which was filled with aqueous NaOH solution. The temperature of the sample vial was controlled using a water bath. After a certain period, the B-ZnO NWA was taken out of the sample vial and rinsed with 20 mL deionized water 3 times. The cleaned B-ZnO NWA was dried and stored in a vacuum drier.

2.4. Characterization

The scanning electron microscope (SEM) images were obtained with a GeminiSEM-500 working in the Inlens-SE mode at 15 kV. The transmission electron microscope (TEM) images were collected with a JEM2100F (JEOL, Japan) with an accelerating voltage of 200 kV. The energy dispersive spectroscopy (EDS) was conducted on the energy dispersive spectrometer equipped on the GeminiSEM-500 (Zeiss, Germany). The X-ray diffraction (XRD) patterns were acquired using a D8 Advance (Bruker, Germany) X-ray diffractometer along with an excitation source of Cu Kα radiation (λ = 1.5418 Å). UV-vis diffuse reflectance spectra were measured on a 2600 UV-vis spectrophotometer (Shimadzu, Japan) equipped with an ISR-2600PLUS integrating sphere (Shimadzu, Japan). BaSO$_4$ powder was used for the baseline measurements. The bandgap energy (E_g) of B-ZnO NWA was calculated using Tauc's equation [17]:

$$(\alpha h v)^n = A\left(h v - E_g\right)$$

where α is the absorption coefficient, h is the Planck constant, v is the frequency of phonon, A is a constant, and n is 2 for ZnO with a direct bandgap. Based on the Kubelka–Munk method [18,19], the absorption coefficient can be expressed as:

$$\alpha = SF(R)/2v_p$$

where S is the scattering coefficient, R is the reflectance, v_p is the volume fraction of absorbing species, and $F(R)$ is the Kubelka-Munk function:

$$F(R) = \frac{(1 - R)^2}{2R}$$

Assuming that S is independent of the frequency of incident light, α is linearly related to $F(R)$. By replacing the α with $F(R)$, Tauc's equation can be rewritten as:

$$(F(R)hv)^2 = B\left(hv - E_g\right)$$

Thus, E_g can be obtained by extrapolating the linear portion of $(F(R)hv)^2$ vs. hv plot to $F(R)hv = 0$.

3. Results

3.1. Controlled Synthesis of Zn NWA

The synthetic process of Zn NWA is schematically illustrated in Figure 1a. During the hot-pressing process, metallic zinc is "squeezed" into the well-aligned nanopores of AAO templates through plastic deformation under high temperature and pressure for 60 min. As confirmed by the XRD patterns (Figure S1), both the Zn foil and Zn NWA are pure zinc (PDF 65-5973). By adjusting the pore size of the AAO templates, Zn NWA with different diameters ranging from 60 nm to 380 nm can be obtained (Figure 1b–d). The length of Zn NWA can be controlled by tuning hot-pressing parameters including the hot-pressing temperature, pressure, and holding time. For instance, the length of Zn NWA increases from 2.5 µm to 11.5 µm as the holding time increases from 20 min to 120 min (Figure 1e–g). For the rest of this study, Zn NWA prepared by using AAO templates with a 200 nm nominal pore size and a holding time of 60 min were used.
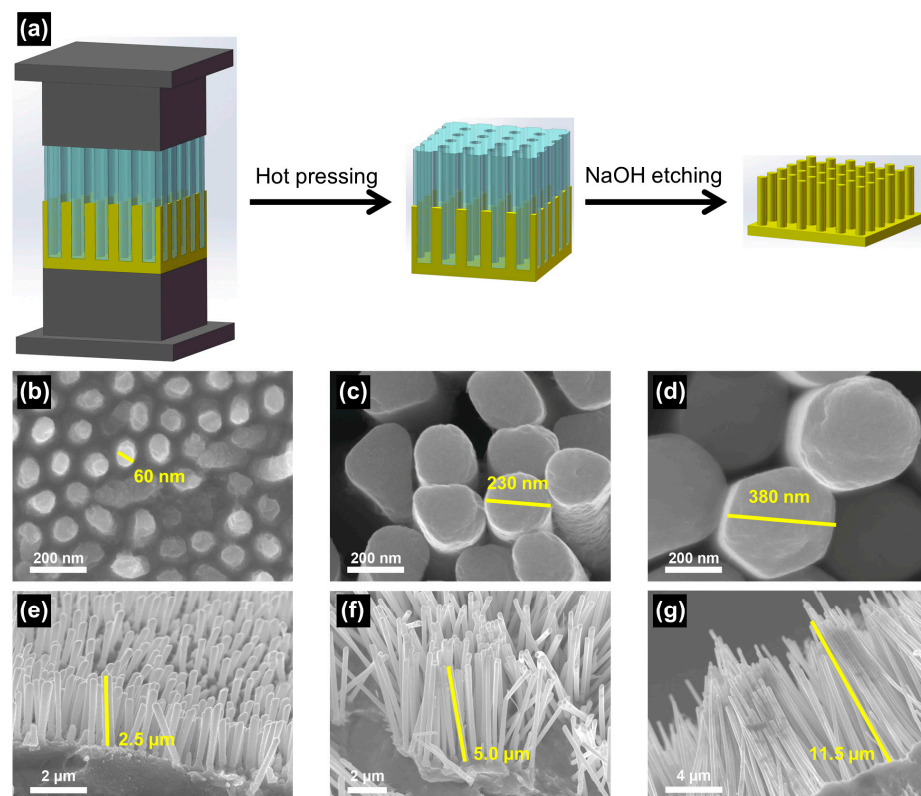

Figure 1. (**a**) Synthetic process of Zn NWA. Zn NWA that is prepared using AAO templates with (**b**) 50 nm, (**c**) 200 nm, and (**d**) 400 nm nominal pore size. Zn NWA that is prepared using a 200 nm AAO template with a hold time of (**e**) 20 min, (**f**) 60 min, and (**g**) 120 min.

3.2. The Effect of NaOH Concentration on the Growth of B-ZnO NWA

B-ZnO NWA is synthesized by immersing the Zn NWA in an aqueous NaOH solution at room temperature for 24 h. After the immersion process, the surface of Zn NWA is decorated with nanorod branches. When the NaOH concentration increases from 0.04 M

to 0.06 M, the size of these branches increases (Figure 2a,b). With the further increase in the NaOH concentration, however, the size of these branches decreases (Figure 2c–f). When the Zn NWA is immersed in 0.2 M NaOH solution, no branches can be observed on the surface of Zn NWA (Figure 2f). The transformation of Zn to ZnO in NaOH solution is confirmed by the diffraction peaks of ZnO in XRD patterns (Figure 2g). When the NaOH concentration increases from 0.04 M to 0.08 M, the relative intensity of the ZnO diffraction peaks increases, indicating the promoted growth of ZnO. With the further increase in the NaOH concentration, the relative intensity of the ZnO diffraction peaks decreases, suggesting that the growth of ZnO is hindered. Based on the SEM images and XRD patterns, it can be determined that these branches are ZnO. The high-resolution TEM (HRTEM) image and the corresponding fast Fourier transformation pattern (FFT) of a branch from the B-ZnO NWA prepared in 0.08 M NaOH solution further corroborate this conclusion (Figure 2h). To promote the growth of ZnO branches, the NaOH concentration should not be too high. The optimal NaOH concentration found in this study is 0.08 M.
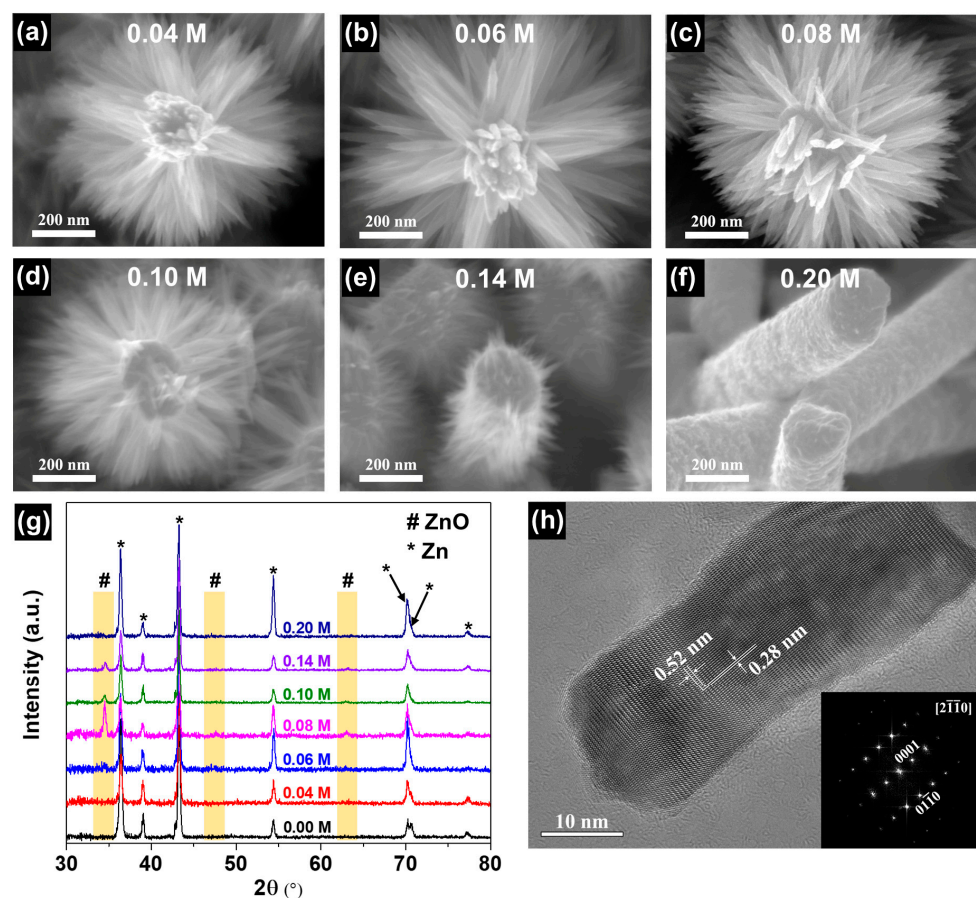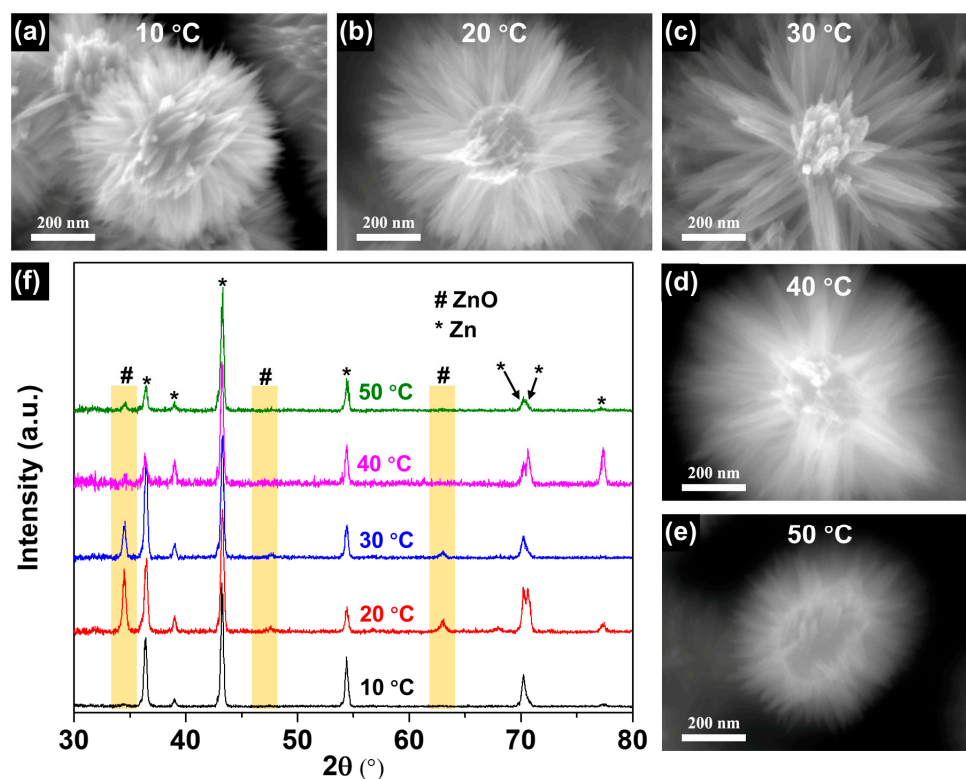

Figure 2. SEM images of B-ZnO NWA prepared in (**a**) 0.04 M, (**b**) 0.06 M, (**c**) 0.08 M, (**d**) 0.10 M, (**e**) 0.14 M, and (**f**) 0.20 M NaOH solution. (**g**) XRD patterns of B-ZnO NWA prepared in NaOH solution with different concentrations. (**h**) HRTEM image of a ZnO branch, the inset is the corresponding FFT pattern.

3.3. The Effect of Solution Temperature on the Growth of B-ZnO NWA

In addition to the NaOH concentration, the solution temperature also affects the growth of B-ZnO NWA. The SEM images of B-ZnO NWA prepared in 0.08 M NaOH solution for 24 h at different temperatures are shown in Figure 3a–e. As the temperature increases from 10 °C to 30 °C, the size of the ZnO branches (Figure 3a–c) increases, indicating the promoted growth of ZnO branches. When the temperature further increases from 30 °C to 50 °C, the size (Figure 3c–e) and the relative intensity of the ZnO diffraction peaks (Figure 3f) decrease, implying that the growth of the ZnO branches is hindered. As a result,

a moderate temperature is required to promote the growth of the ZnO branches. For the convenience of preparation and cost reduction, room temperature (25 °C) is selected for the synthesis of B-ZnO NWA.

Figure 3. SEM images of B-ZnO NWA prepared at (**a**) 10 °C, (**b**) 20 °C, (**c**) 30 °C, (**d**) 40 °C, and (**e**) 50 °C. (**f**) XRD patterns of B-ZnO NWA prepared at different temperatures.

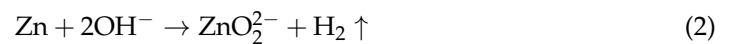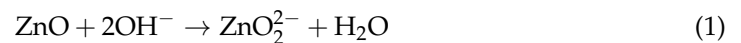*3.4. The Effect of Immersion Time on the Growth of B-ZnO NWA*

To obtain more insights into the growth of B-ZnO NWA, the morphology evolution of B-ZnO NWA prepared in 0.08 M NaOH solution at room temperature with different immersion times is investigated. The surface of pristine Zn NWA is relatively smooth (Figure 4a). After 1 h immersion, the surface of Zn NWA is covered with nanoparticles (Figure 4b). As the immersion time increases to 2 h, numerous ZnO branches grow on the surface of Zn NWA (Figure 4c). With a further increase in immersion time, the size of the ZnO branches gradually increases (Figure 4i) along with a decrease in the density of B-ZnO NW (Figures S2 and S3). In the meantime, the relative intensity of the ZnO diffraction peaks also increases as the immersion time increases (Figure 4j). These results confirm the continuous growth of the ZnO branches. The EDS analysis shows that the O/Zn ratio of B-ZnO NWA increases as the immersion time increases. After 36 h, the O/Zn ratio was close to unity (inset of Figure 4i), indicating that most of the Zn NWA was transformed to B-ZnO NWA.
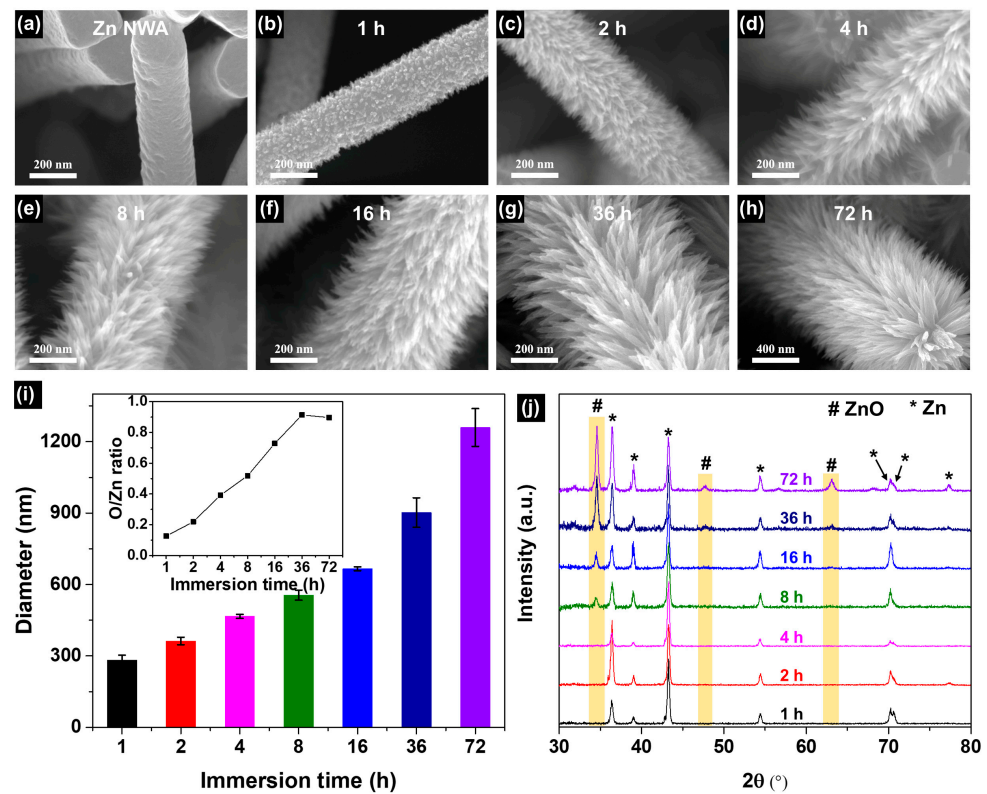
Figure 4. SEM images of (**a**) Zn NWA and B-ZnO NWA prepared in 0.08 M NaOH solution with an immersion time of (**b**) 1 h, (**c**) 2 h, (**d**) 4 h, (**e**) 8 h, (**f**) 16 h, (**g**) 36 h, and (**h**) 72 h. (**i**) Diameter of B-ZnO NW prepared with different immersion times. The corresponding O/Zn ratio of B-ZnO NWA is given as an inset. (**j**) XRD patterns of B-ZnO NWA prepared with different immersion times.

4. Discussion

Based on the experimental results, the growth mechanism of B-ZnO NWA is explained below. When Zn NWA is immersed in NaOH solution, three possible reactions may occur [20,21]:

$$ZnO + 2OH^- \rightarrow ZnO_2^{2-} + H_2O \tag{1}$$

$$Zn + 2OH^- \rightarrow ZnO_2^{2-} + H_2 \uparrow \tag{2}$$

$$ZnO_2^{2-} + H_2O \rightarrow ZnO + 2OH^- \tag{3}$$

Firstly, the native oxide of Zn NWA is corroded by the NaOH solution through reaction (1). When parts (especially defective sites with higher energy) of the native oxide are etched away, the Zn core will be exposed. Then, the corrosion of Zn becomes dominant through reaction (2), thereby further increasing the local concentration of ZnO_2^{2-} around the Zn NW. When the local concentration is oversaturated, the excess ZnO_2^{2-} will react with the water and produce ZnO via reaction (3) [22]. Due to the relatively higher concentration of ZnO_2^{2-} around Zn NW, ZnO will preferentially precipitate on Zn NW, resulting in the growth of ZnO branches. With a similar composition and structure, the native oxide of Zn NW, therefore, will serve as the substrate for the growth of ZnO branches [6].

The structure of Zn NWA is vital to the growth of ZnO branches and the formation of B-ZnO NWA because the confined space between Zn NW can hinder the diffusion and, thus, promote the oversaturation of ZnO_2^{2-}. To illustrate the effect of the diffusion of ZnO_2^{2-} on the growth of ZnO branches, a piece of Zn foil was immersed in 0.1 M NaOH solution at 25 °C for 24 h. As shown in Figure 5, ZnO NWA was found on the back surface (in contact with the bottom of the sample vial) instead of the front surface. This phenomenon is mainly ascribed to the enhanced diffusion on the front surface with more open space, which impedes the emergence of ZnO_2^{2-} oversaturation.
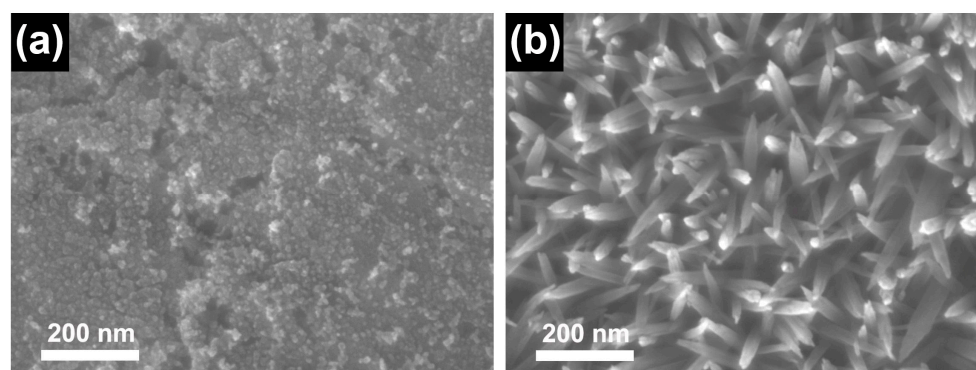
Figure 5. SEM images of Zn foil immersed in 0.1 M NaOH at 25 °C for 24 h. (**a**) Front surface. (**b**) Back surface.

In dilute NaOH solution (0.04 M–0.08 M), the corrosion of ZnO through reaction (1) is slow and negligible. In this situation, the growth of ZnO branches through reaction (3) is mainly governed by the rate of reaction (2). As the NaOH concentration increases from 0.04 M to 0.08 M, the rate of reaction (2) increases, leading to a higher local concentration of ZnO_2^{2-} [23] and thus promoting the growth of ZnO branches. In concentrated NaOH solution (0.08 M–0.20 M), the corrosion of ZnO through reaction (1) is severe. When the NaOH concentration further increases from 0.08 M to 0.2 M, the enhanced corrosion of ZnO hinders the growth of ZnO branches. The inhibition of the growth of ZnO nanorods was also found in concentrated ammonia solution [24].

The effect of temperature on the growth of B-ZnO NWA is similar to that of the NaOH concentration. At low temperatures (10 °C–30 °C), the corrosion of ZnO through reaction (1) is slow. In this case, the increased temperature will facilitate the growth of ZnO by accelerating reaction (2) and (3). With the further increase in the temperature (30 °C–50 °C), the growth of ZnO branches is hindered, likely due to the enhanced dissolution of ZnO at higher temperatures [25].

In the initial stage of the growth of ZnO branches, the dissolution of Zn through reaction (2) provides plenty of ZnO_2^{2-}, which promotes the growth of ZnO branches. Due to the filling of the void space between B-ZnO NW by the growth of ZnO branches, the volume filling ratio of B-ZnO NWA gradually increases. When all metallic zinc precursors are consumed or adjacent B-ZnO NW come into contact (Figure S4), the further growth of ZnO branches will be limited by the shortage of ZnO_2^{2-} or confined space. Under this circumstance, the morphology evolution of B-ZnO NWA will turn to be controlled by the Ostwald ripening process towards a lower system energy state [26–28]. Some energetically less favorable B-ZnO NW will be dissolved via reaction (1) or (2), whose products, i.e., ZnO_2^{2-}, will further promote the growth of those energetically more favorable B-ZnO NWA. As a result, the size of the ZnO branches increases, and the density of B-ZnO NW decreases as immersion time increases.

A unique feature that distinguishes our B-ZnO NWA from those reported previously is the hollow trunks (Figure 6). During the growth of ZnO branches through reaction (3), the ZnO_2^{2-} precursors are mainly from the corrosion of Zn NW, hence the mass transfer of Zn proceeds radially from the inside out. As Zn atoms diffuse from the core to the surface, the corresponding vacancies diffuse in the opposite direction. To minimize the total energy, these vacancies tend to agglomerate, forming clusters and gradually developing into large cavities [29,30] inside the Zn NW. Due to the geometric symmetry, these cavities usually situate at the center of the Zn NW (Figure 6). Compared to the B-ZnO NWA with dense trunks, the hollow trunks will further increase the specific area of the B-ZnO NWA prepared herein [31].
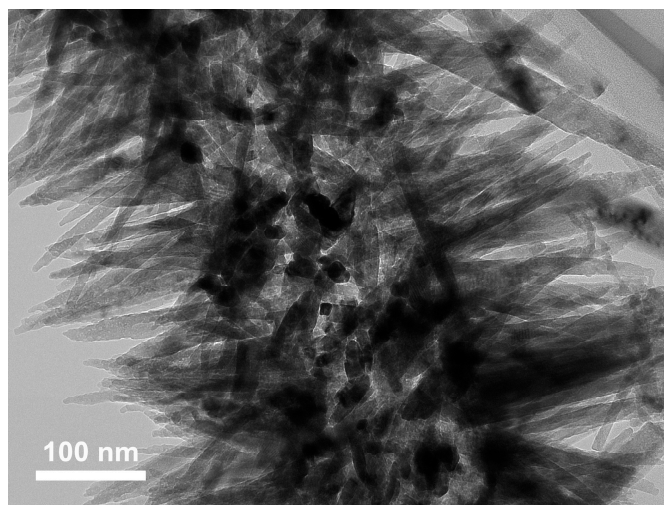
Figure 6. TEM image of B-ZnO NW prepared in 0.08 M NaOH solution at 25 °C for 24 h.

It is worth noting that the top of the ZnO branches is tapered (Figures 6 and S5). The formation of this morphology is deemed to arise from the concentration gradient of the ZnO_2^{2-} precursor. During the growth of the ZnO branches, ZnO_2^{2-} is mainly supplied by the corrosion of Zn NW. Thus, there is a concentration gradient from the surface of Zn NW to the tip of the ZnO branches [22,24]. This concentration gradient is further enlarged by the enhanced diffusion due to the large space around the tip of the ZnO branches. Therefore, the growth rate decreases from the root to the tip of ZnO branches, leading to the formation of the tapered tip.

According to Tauc's plot, the bandgap of B-ZnO NWA is determined to be 3.29 eV (Figure 7a), which is close to the value of other ZnO nanomaterials [18]. Due to the wide bandgap, B-ZnO NWA shows strong adsorption in the UV region of the UV-vis diffuse reflectance spectrum (Figure 7b). Compared to ZnO NWA without secondary branches (inset with a blue outline in Figure 7b), B-ZnO NWA shows significantly lower reflectance in the visible region. The decreased reflectance is mainly attributed to the strong light scattering within the hierarchical nanostructure of B-ZnO NWA. The incident light is trapped by the multiple reflections among the dense branches and trunks of B-ZnO NWA, which increases the propagation path and reduces the reflection. The great light-trapping ability is highly conducive to the application of B-ZnO NWA in photovoltaics [32] or photochemistry [9].
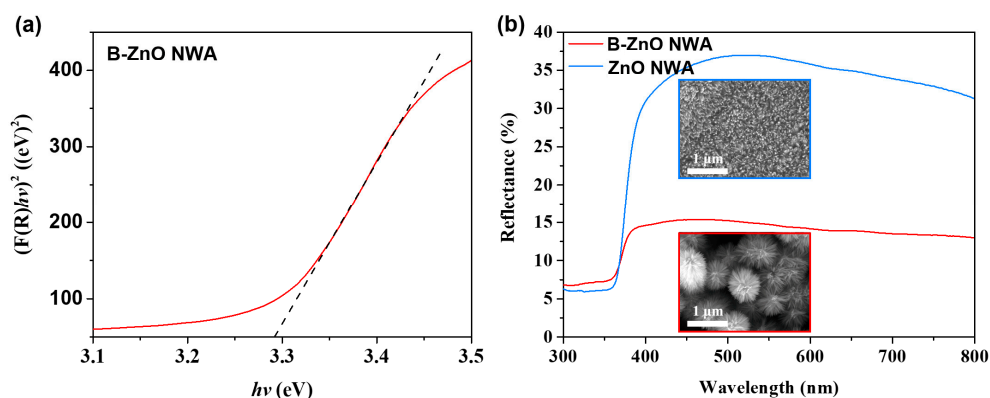
Figure 7. (**a**) Tauc's plot of B-ZnO NWA. (**b**) UV-vis diffuse reflectance spectra of B-ZnO NWA and ZnO NWA.

5. Conclusions

In summary, we developed a novel method for the facile synthesis of B-ZnO NWA via the immersion of Zn NWA in NaOH solution at room temperature. The growth of B-ZnO NWA is achieved through the corrosion of Zn NWA to produce ZnO_2^{2-} precursors, which hydrolyze into ZnO with the necessary oversaturation. The morphology of B-ZnO NWA can be controlled by tuning the morphology of Zn NWA or adjusting the NaOH concentration, corrosion temperature, and corrosion time. The morphology of ZnO NWA depends on the pore structure of the AAO templates and hot-pressing parameters. With the increase in NaOH concentration or corrosion temperature, the growth of ZnO branches is first promoted and then hindered. The increased corrosion time leads to an increased size of ZnO branches and a higher volume filling ratio of B-ZnO NWA. Due to the out-diffusion of Zn from the core of Zn NW during the growth of ZnO branches, B-ZnO NWA has hollow trunks, which can further increase the specific area of B-ZnO NWA. The hierarchical structure enables multireflection of incident light within B-ZnO NWA and, thus, significantly reduces the reflectance in the visible region. Considering the environmentally friendliness, low cost, and simplicity of the synthesis, together with the tunable morphology, B-ZnO NWA prepared herein are promising candidates for various applications, especially those related to the conversion and utilization of solar energy, which are gaining increasing interest nowadays.

References

1. Kegel, J.; Povey, I.M.; Pemble, M.E. Zinc oxide for solar water splitting: A brief review of the material's challenges and associated opportunities. *Nano Energy* **2018**, *54*, 409–428. [CrossRef]
2. Look, D.C. Recent advances in ZnO materials and devices. *Mater. Sci. Eng. B* **2001**, *80*, 383–387. [CrossRef]
3. Xu, S.; Wang, Z.L. One-dimensional ZnO nanostructures: Solution growth and functional properties. *Nano Res.* **2011**, *4*, 1013–1098. [CrossRef]
4. Dong, Y.; Zhu, X.; Pan, F.; Deng, B.; Liu, Z.; Zhang, X.; Huang, C.; Xiang, Z.; Lu, W. Mace-like carbon fiber/ZnO nanorod composite derived from Typha orientalis for lightweight and high-efficient electromagnetic wave absorber. *Adv. Compos. Hybrid Mater.* **2021**, *4*, 1002–1014. [CrossRef]
5. Ebrahimi, M.; Yousefzadeh, S.; Samadi, M.; Dong, C.; Zhang, J.; Moshfegh, A.Z. Facile preparation of branched hierarchical ZnO nanowire arrays with enhanced photocatalytic activity: A photodegradation kinetic model. *Appl. Surf. Sci.* **2018**, *435*, 108–116. [CrossRef]
6. McCune, M.; Zhang, W.; Deng, Y. High Efficiency Dye-Sensitized Solar Cells Based on Three-Dimensional Multilayered ZnO Nanowire Arrays with "Caterpillar-like" Structure. *Nano Lett.* **2012**, *12*, 3656–3662. [CrossRef]

7. Ko, S.H.; Lee, D.; Kang, H.W.; Nam, K.H.; Yeo, J.Y.; Hong, S.J.; Grigoropoulos, C.P.; Sung, H.J. Nanoforest of Hydrothermally Grown Hierarchical ZnO Nanowires for a High Efficiency Dye-Sensitized Solar Cell. *Nano Lett.* **2011**, *11*, 666–671. [CrossRef]
8. Bai, Z.; Yan, X.; Li, Y.; Kang, Z.; Cao, S.; Zhang, Y. 3D-Branched ZnO/CdS Nanowire Arrays for Solar Water Splitting and the Service Safety Research. *Adv. Energy Mater.* **2016**, *6*, 1501459. [CrossRef]
9. Ren, X.; Sangle, A.; Zhang, S.; Yuan, S.; Zhao, Y.; Shi, L.; Hoye, R.L.Z.; Cho, S.; Li, D.; MacManus-Driscoll, J.L. Photoelectrochemical water splitting strongly enhanced in fast-grown ZnO nanotree and nanocluster structures. *J. Mater. Chem. A* **2016**, *4*, 10203–10211. [CrossRef]
10. Zhang, Y.; Xu, J.; Xiang, Q.; Li, H.; Pan, Q.; Xu, P. Brush-Like Hierarchical ZnO Nanostructures: Synthesis, Photoluminescence and Gas Sensor Properties. *J. Phys. Chem. C* **2009**, *113*, 3430–3435. [CrossRef]
11. An, S.; Park, S.; Ko, H.; Jin, C.; Lee, W.I.; Lee, C. Enhanced gas sensing properties of branched ZnO nanowires. *Thin Solid Film* **2013**, *547*, 241–245. [CrossRef]
12. Zhao, F.; Zheng, J.-G.; Yang, X.; Li, X.; Wang, J.; Zhao, F.; Wong, K.S.; Liang, C.; Wu, M. Complex ZnO nanotree arrays with tunable top, stem and branch structures. *Nanoscale* **2010**, *2*, 1674–1683. [CrossRef]
13. Choi, J.; Ji, H.; Tambunan, O.T.; Hwang, I.-S.; Woo, H.-S.; Lee, J.-H.; Lee, B.W.; Liu, C.; Rhee, S.J.; Jung, C.U.; et al. Brush-Shaped ZnO Heteronanorods Synthesized Using Thermal-Assisted Pulsed Laser Deposition. *ACS Appl. Mater. Interfaces* **2011**, *3*, 4682–4688. [CrossRef] [PubMed]
14. Sun, X.; Li, Q.; Jiang, J.; Mao, Y. Morphology-tunable synthesis of ZnO nanoforest and its photoelectrochemical performance. *Nanoscale* **2014**, *6*, 8769–8780. [CrossRef] [PubMed]
15. Bielinski, A.R.; Boban, M.; He, Y.; Kazyak, E.; Lee, D.H.; Wang, C.; Tuteja, A.; Dasgupta, N.P. Rational Design of Hyperbranched Nanowire Systems for Tunable Superomniphobic Surfaces Enabled by Atomic Layer Deposition. *ACS Nano* **2017**, *11*, 478–489. [CrossRef] [PubMed]
16. Luan, C.; Shao, Y.; Lu, Q.; Gao, S.; Huang, K.; Wu, H.; Yao, K. High-Performance Carbon Dioxide Electrocatalytic Reduction by Easily Fabricated Large-Scale Silver Nanowire Arrays. *ACS Appl. Mater. Interfaces* **2018**, *10*, 17950–17956. [CrossRef]
17. Tauc, J.; Grigorovici, R.; Vancu, A. Optical Properties and Electronic Structure of Amorphous Germanium. *Phys. Status Solidi B* **1966**, *15*, 627–637. [CrossRef]
18. Senthilkumar, N.; Nandhakumar, E.; Priya, P.; Selvakumar, M.; Potheher, I.V. Green and sustainable preparation of flower-like ZnO nanostructures via soft bio-template approach for the enhancement of biomedical applications. *Appl. Phys. A* **2021**, *128*, 78. [CrossRef]
19. Nobbs, J.H. Kubelka—Munk Theory and the Prediction of Reflectance. *Rev. Prog. Color. Relat. Top.* **1985**, *15*, 66–75. [CrossRef]
20. Fang, Y.; Pang, Q.; Wen, X.; Wang, J.; Yang, S. Synthesis of Ultrathin ZnO Nanofibers Aligned on a Zinc Substrate. *Small* **2006**, *2*, 612–615. [CrossRef]
21. Cho, S.; Jang, J.-W.; Lee, J.S.; Lee, K.-H. Room temperature synthesis and optical properties of small diameter (5 nm) ZnO nanorod arrays. *Nanoscale* **2010**, *2*, 2199–2202. [CrossRef] [PubMed]
22. Tan, W.K.; Razak, K.A.; Lockman, Z.; Kawamura, G.; Muto, H.; Matsuda, A. Formation of highly crystallized ZnO nanostructures by hot-water treatment of etched Zn foils. *Mater. Lett.* **2013**, *91*, 111–114. [CrossRef]
23. Kar, S.; Dev, A.; Chaudhuri, S. Simple Solvothermal Route to Synthesize ZnO Nanosheets, Nanonails, and Well-Aligned Nanorod Arrays. *J. Phys. Chem. B* **2006**, *110*, 17848–17853. [CrossRef] [PubMed]
24. Li, Z.; Huang, X.; Liu, J.; Li, Y.; Ji, X.; Li, G. Growth and comparison of different morphologic ZnO nanorod arrays by a simple aqueous solution route. *Mater. Lett.* **2007**, *61*, 4362–4365. [CrossRef]
25. Peterson, R.B.; Fields, C.L.; Gregg, B.A. Epitaxial Chemical Deposition of ZnO Nanocolumns from NaOH Solutions. *Langmuir* **2004**, *20*, 5114–5118. [CrossRef] [PubMed]
26. Liu, X.; Huang, W.; Huang, G.; Fu, F.; Cheng, H.; Guo, W.; Li, J.; Wu, H. Synthesis of bilayer ZnO nanowire arrays: Morphology evolution, optical properties and photocatalytic performance. *Ceram. Int.* **2015**, *41*, 11710–11718. [CrossRef]
27. Li, Z.; Huang, X.; Liu, J.; Ai, H. Single-crystalline ZnO nanowires on zinc substrate by a simple hydrothermal synthesis method. *Mater. Lett.* **2008**, *62*, 2507–2511. [CrossRef]
28. Tong, Y.; Liu, Y.; Dong, L.; Zhao, D.; Zhang, J.; Lu, Y.; Shen, D.; Fan, X. Growth of ZnO Nanostructures with Different Morphologies by Using Hydrothermal Technique. *J. Phys. Chem. B* **2006**, *110*, 20263–20267. [CrossRef]
29. Wang, X.; Hatzoglou, C.; Sneed, B.; Fan, Z.; Guo, W.; Jin, K.; Chen, D.; Bei, H.; Wang, Y.; Weber, W.J.; et al. Interpreting nanovoids in atom probe tomography data for accurate local compositional measurements. *Nat. Commun.* **2020**, *11*, 1022. [CrossRef]
30. Ortega, Y.; Dieker, C.; Jäger, W.; Piqueras, J.; Fernández, P. Voids, nanochannels and formation of nanotubes with mobile Sn fillings in Sn doped ZnO nanorods. *Nanotechnology* **2010**, *21*, 225604. [CrossRef]
31. Yu, H.; Zhang, Z.; Han, M.; Hao, X.; Zhu, F. A General Low-Temperature Route for Large-Scale Fabrication of Highly Oriented ZnO Nanorod/Nanotube Arrays. *J. Am. Chem. Soc.* **2005**, *127*, 2378–2379. [CrossRef] [PubMed]
32. Hsieh, M.-Y.; Kuo, S.-Y.; Han, H.-V.; Yang, J.-F.; Liao, Y.-K.; Lai, F.-I.; Kuo, H.-C. Enhanced broadband and omnidirectional performance of Cu(In,Ga)Se$_2$ solar cells with ZnO functional nanotree arrays. *Nanoscale* **2013**, *5*, 3841–3846. [CrossRef] [PubMed]